arXiv:astro-ph/9705138v1 19 May 1997

Periodic Orbits in Triaxial Galaxies with Weak Cusps

Tema Fridman and David Merritt
Department of Physics and Astronomy, Rutgers University, New Brunswick, NJ 08855

ABSTRACT

The orbital structure of triaxial models with weak central density cusps, $\rho \propto r^{-\gamma}$, $\gamma < 1$, is investigated. The stability of the x- (long-) axis orbit – and hence the existence of box orbits – depends sensitively on γ; the range of model shapes for which the x-axis orbit is stable becomes progressively smaller as γ approaches one. The banana and fish boxlets in the $x-z$ (long axis–short axis) plane are stable over a wide range of model parameters. The boxlets in the $x-y$ and $y-z$ planes are generally vertically unstable.

1. Introduction

The phase space of Stäckel potentials is completely occupied by four major families of regular orbits: the boxes, and the three families of tubes (Kuzmin 1973; de Zeeuw & Lynden-Bell 1985). Roughly the same is true in many nonrotating triaxial potentials corresponding to mass models with smooth cores: most of the orbits have shapes that can be identified with one of the four families of regular orbits in Stäckel potentials (Schwarzschild 1979). However the situation is very different in triaxial models with divergent central densities, or cusps. While the tube orbits are not strongly affected by cusps, the boxlike orbits – orbits with stationary points and filled centers – are often rendered stochastic, except when they are associated with a resonant orbit that avoids the center (Gerhard & Binney 1985; Lees & Schwarzschild 1992; Merritt & Fridman 1996; Papaphilippou & Laskar 1997).

Kormendy pointed out already in 1985 that many early-type galaxies and bulges have central brightness profiles that deviate slightly but systematically from that of an isothermal core. The significance of this deviation was not recognized for ten more years, however, due to an optical illusion associated with projection onto the plane of the sky. A luminosity density profile that varies as $r^{-\gamma}$ at small radii generates a power-law cusp in projection only if $\gamma > 1$. When $\gamma = 1$, the surface brightness exhibits a curving, logarithmically-divergent central profile (e.g. Dehnen 1993, Fig. 1), and for $\gamma < 1$ the central surface brightness is finite. The observed brightness profile of a galaxy like M87, which has a cusp with $\gamma \approx 0.8$

(Lauer et al. 1992), differs only subtly from that of a galaxy with an isothermal core (Kormendy 1985). This is true in spite of the fact that the cusp in M87 is well resolved from the ground.

Thus even if galaxies were distributed uniformly over γ, their central brightness profiles would appear to fall into one of two distinct categories: the "cores" ($\gamma \leq 1$) and the "power-laws" ($\gamma > 1$). Just such a dichotomy was proposed following the first nuclear brightness measurements from HST (Ferrarese et al. 1994; Lauer et al. 1995). Merritt & Fridman (1995) suggested that the centers of *all* early-type galaxies, including the core galaxies, might contain power law cusps in the space density. They used a nonparametric deprojection algorithm to confirm this hypothesis for six galaxies observed with HST. Gebhardt et al. (1996) subsequently reanalyzed the full sample of 42 early-type galaxies observed by Lauer et al. (1995) and verified the power-law nature of the deprojected cusps in each case. They also confirmed a tendency, noted earlier by Kormendy (1985), for the brightest galaxies to have the shallowest cusps.

Most of the theoretical work on orbital motion in triaxial potentials has focused on mass models with cores, $\gamma = 0$, or with steep cusps, $\gamma = 2$. But galaxies with cores probably do not exist; and only the faintest ellipticals, $M_v \gtrsim -19$, have cusps that are predictably as steep as r^{-2}. Here we present the first detailed study of periodic orbits in triaxial models with weak cusps, $0 \leq \gamma < 1$, characteristic of bright elliptical galaxies. The value $\gamma = 1$ is a natural one for separating "weak" from "strong" cusps, since a central density that increases more rapidly than r^{-1} implies a divergent central force. For instance, a spherical galaxy with Dehnen's (1993) density law

$$\rho(r) = \frac{(3-\gamma)M}{4\pi a^3}\left(\frac{r}{a}\right)^{-\gamma}\left(1+\frac{r}{a}\right)^{-(4-\gamma)} \tag{1}$$

has a gravitational force

$$-\frac{\partial\Phi}{\partial r} = -\frac{GM}{a^2}\left(\frac{r}{a}\right)^{1-\gamma}\left(1+\frac{r}{a}\right)^{\gamma-3}. \tag{2}$$

Dehnen's law, with $\gamma = 2$ (Jaffe 1983) and $\gamma = 1$ (Hernquist 1990), has been shown to accurately describe the brightness profiles of a number of early-type galaxies. The triaxial generalization of Dehnen's law,

$$\rho(m) = \frac{(3-\gamma)}{4\pi abc} m^{-\gamma}(1+m)^{-(4-\gamma)}, \tag{3}$$

$$m^2 = \frac{x^2}{a^2} + \frac{y^2}{b^2} + \frac{z^2}{c^2}, \quad a \geq b \geq c \geq 0, \tag{4}$$

was presented by Merritt & Fridman (1996), who derived expressions for the gravitational potential, force and force gradients for $0 \leq \gamma \leq 2$.

Our primary concern here is with the closed "boxlets", the low-order resonant orbits that act as parents of the boxlike orbits in non-integrable triaxial potentials. Most important is the x- (long-) axis orbit, which generates the box orbits in Stäckel potentials. Its instability usually occurs through the bifucation of a $2:1$ resonant orbit, or "banana." (We adopt Miralda-Escudé & Schwarzschild's (1989) scheme for labeling the closed boxlets; their Figure 4 illustrates the different types.) Higher-order resonances produce the "fish" $(3:2)$ and "pretzel" $(4:3)$ orbits. Boxlets corresponding to each resonance are expected to exist in all three of the principal planes of a triaxial model, at least at certain energies and for certain values of the model axis ratios. However little is known about the dependence of boxlet stability on model parameters. In particular, the vertical stability of the closed boxlets has been very little explored.

In the present paper, we locate and test the stability of the axial orbits, the bananas, and the fish as a function of the three parameters that define Dehnen's models: the cusp slope γ; the short-to-long axis ratio c/a; and the degree of triaxiality, expressed in terms of $T = (a^2 - b^2)/(a^2 - c^2)$. $T = 0$ corresponds to oblate-axisymmetry, and $T = 1$ to prolate-axisymmetry. For each set of model parameters, we present results as a function of energy; thus we explore a four-dimensional parameter space for each of the orbit families. A total of approximately 3.5×10^4 orbits were investigated. The numerical scheme for evaluating the stability of the boxlets is presented in §2. The results for the axial orbits, the bananas and the fish are presented in §3, 4 and 5 respectively. Our results are summarized in §6.

There is increasingly strong evidence for dark mass concentrations, possibly supermassive black holes, at the centers of many early-type galaxies (Kormendy & Richstone 1995). We ignore the (possibly substantial) effect that such singularities would have on the behavior of boxlike orbits: partly because the universality of central black holes has not yet been established; and partly because the behavior of orbits in triaxial galaxies with cusps provides an essential first step toward understanding the additional effects of a central black hole.

2. Linear Stability Analysis

We applied a numerical version of the standard Floquet-Liapunov theory (Floquet 1883; Liapunov 1892) to evaluate the stability of the lowest-order periodic orbits in Dehnen's

model potential. Our approach was similar to that of earlier studies (e.g. Magnenat 1982; Pfenniger 1984), with one difference. Instead of integrating a set of orbits whose initial conditions were offset by small, finite amounts from those of the closed orbit, we integrated the linearized equations corresponding to a set of infinitesimal perturbations about the closed orbit. Our results are therefore strictly independent of the numerical amplitude of the perturbation.

Let $\mathbf{X}(t)$, $\mathbf{V}(t)$ be the parametric representation of a closed orbit. The equations of motion are

$$\frac{d\mathbf{X}(t)}{dt} = \mathbf{V}(t), \quad \frac{d\mathbf{V}(t)}{dt} = -\nabla\Phi(\mathbf{X}). \tag{5}$$

A nearby orbit has coordinates $\mathbf{X}(t) + \mathbf{x}(t)$, $\mathbf{V}(t) + \mathbf{v}(t)$. For small $\mathbf{x}$ and $\mathbf{v}$, the equations of motion are

$$\begin{aligned} \frac{d(\mathbf{X}+\mathbf{x})}{dt} &= \mathbf{V} + \mathbf{v}, \\ \frac{d(\mathbf{V}+\mathbf{v})}{dt} &= -\nabla\Phi(\mathbf{X}+\mathbf{x}) \approx -\nabla\Phi(\mathbf{X}) + (\mathbf{x}\nabla)(\nabla\mathbf{\Phi}(\mathbf{X})). \end{aligned} \tag{6}$$

Subtracting equations (5) from equations (7), we have

$$\frac{d\mathbf{x}}{dt} = \mathbf{v}, \quad \frac{d\mathbf{v}}{dt} = -(\mathbf{x}\nabla)(\nabla\Phi(\mathbf{X})), \tag{7}$$

or

$$\frac{d}{dt}\begin{pmatrix} x \\ y \\ z \\ v_x \\ v_y \\ v_z \end{pmatrix} = -\begin{pmatrix} 0 & 0 & 0 & -1 & 0 & 0 \\ 0 & 0 & 0 & 0 & -1 & 0 \\ 0 & 0 & 0 & 0 & 0 & -1 \\ \Phi_{xx} & \Phi_{xy} & \Phi_{xz} & 0 & 0 & 0 \\ \Phi_{xy} & \Phi_{yy} & \Phi_{yz} & 0 & 0 & 0 \\ \Phi_{xz} & \Phi_{yz} & \Phi_{zz} & 0 & 0 & 0 \end{pmatrix}\begin{pmatrix} x \\ y \\ z \\ v_x \\ v_y \\ v_z \end{pmatrix}. \tag{8}$$

The second derivatives of the potential, Φ_{ij}, are taken along the closed orbit whose period is P. Expressions for the Φ_{ij} are given by Merritt & Fridman (1996). The stability of the closed orbit is then determined by the eigenvalues of the monodromy matrix $\mathbf{W}$, where

$$\mathbf{x}(t+P) = \mathbf{W}\mathbf{x}(t) \tag{9}$$

and $\mathbf{x}$ has been redefined to include velocities. We computed the elements of $\mathbf{W}$ by numerically integrating the six linearized equations of motion (8), starting from unit perturbations in each of the coordinates. A 7/8th order, variable timestep integrator – the routine DOPRI8 of Hairer et al. (1987) – was used. Initial conditions for the non-axial

closed orbits were found by an iterative Newton method, and precise orbital periods were calculated using the scheme of Hénon (1982).

Two of the eigenvalues of $\mathbf{W}$ are guaranteed to be unity; these correspond to eigenvectors lying along the closed orbit. The remaining four eigenvalues satisfy $\lambda_1 = 1/\lambda_2$, $\lambda_3 = 1/\lambda_4$; the stability of the closed orbit is determined by the parameters $b_1 = -(\lambda_1 + \lambda_2)$, $b_2 = -(\lambda_3 + \lambda_4)$, with $|b_i| \geq 2$ denoting instability (Broucke 1969). For orbits that lie in a symmetry plane, b_1 and b_2 correspond to perturbations in the orbital plane and perpendicular to the orbital plane, or vice versa. For the simplest orbits, the full set of six perturbation equations is not required; for instance, the stability of the axial orbits can be evaluated using just four independent perturbations.

Axial orbits presented one complication, however. While the gravitational force $-\nabla\Phi$ is everywhere finite in Dehnen models with $\gamma < 1$, the second derivatives of the potential diverge at the origin as $\Phi_{ii} \propto |x_i|^{-\gamma}$. To avoid this divergence, analytical expressions were derived for the evolution of the perturbations very near the origin, allowing this region to be excluded from the numerical integrations.

The accuracy of the algorithms was checked in a number of ways. The monodromy matrix and its eigenvalues were checked to see that they accurately satisfied all of their known, exact properties, e.g. $\det \mathbf{W} = 1$, $\lambda_1 = 1/\lambda_2$, etc. Integrations using an algorithm based on finite-amplitude perturbations were carried out for some orbits and compared to the results of the linearized code. Finally, numerical surfaces of section were constructed for a few models and compared to the results from the stability calculations.

All orbits in a given model were assigned energies from a discrete grid, consisting of 20 energy values that corresponded to the values of the potential on the x-axis of a set of ellipsoidal shells – with the same axis ratios as the density – that divide the model into 21 sections of equal mass. Thus, shell 1 encloses 1/21 of the total mass, shell 2 encloses 2/21, etc. Henceforth units are adopted such that $G = M = a = 1$.

3. Axial Orbits

The long- (x-) axis orbit is stable at all energies in integrable triaxial potentials and acts as the parent of the box orbits (Kuzmin 1973; de Zeeuw & Lynden-Bell 1985). In more general triaxial potentials, like the ones considered here, the x-axis orbit becomes unstable at high energies when its frequency of oscillation falls to 1/2 the average oscillation frequency of a perturbation in the direction of the short or intermediate axis (Miralda-Escudé & Schwarzschild 1989). A bifurcation then occurs, with the $2:1$ $x-z$ or $x-y$ banana orbit

branching off. A similar bifurcation occurs from the intermediate (y-) axis orbit, producing the $y-z$ banana.

Nearer the center, the y- and z-axis orbits become unstable at the bifurcation points of the $1:1$ loop orbits. In models with a harmonic core, the loop orbits first appear just outside of the core (Merritt & de Zeeuw 1982). The $x-y$ loop is the parent of the short-axis tubes, and the $y-z$ loop is the parent of the long-axis tubes. The $x-z$ loop is generally unstable and generates no families of regular orbits (Heiligman & Schwarzschild 1979). In models without cores, the loops and their associated tube orbits may exist all the way into the center.

Figures 1 and 2 display the stability diagrams for the x- and y- axis orbits in Dehnen's potential, for three values of T and four values of γ; a total of 4104 orbits are displayed in each figure. Four cases are distinguished: stability ($\bullet$); instability in the direction of the longer ($+$) or shorter ($\times$) of the two remaining axes; and instability in both directions ($\cdot$).

The x-axis orbit is stable at low energies in all models that are not too highly elongated. As γ increases above zero, the range of model shapes for which the x-axis orbit is stable to the $x-z$ banana bifurcation becomes narrower, eventually including only nearly spherical models (Figure 3). For instance, when $\gamma = 0.9$, the x-axis orbit is stable at the half-mass radius for $c/a \gtrsim 0.8$. Thus, bona-fide box orbits (which require for their existence a stable long-axis orbit) will occur at a wide range of energies only in models that are nearly spherical, that have very weak cusps, or both. Figure 4 illustrates how the bifurcation of the $x-z$ banana orbit takes place at successively lower energies as γ is increased.

As c/a is decreased still more, a second $2:1$ bifurcation from the x-axis orbit sometimes occurs in the direction of the intermediate axis, giving rise to the $x-y$ bananas. Following this bifurcation, the x-axis orbit is unstable in both directions. As Figure 1 shows, the $x-y$ banana bifurcation occurs most readily in nearly prolate models (e.g. $T = 0.8$) in which the y and z axes are nearly equal in length. For nearly oblate models, e.g. $T = 0.2$, the x and y axes are too similar in length for the $x-y$ frequency ratio to ever reach the required value of $2:1$, and the $x-y$ banana does not appear.

Interestingly, the x-axis orbit can again become stable when c/a is made smaller still – typically less than about 0.45. The return to stability coincides with the appearance of the $x-z$ "anti-banana" orbit, a $2:1$ resonant orbit that passes through the center (Miralda-Escudé & Schwarzschild 1989). In nearly oblate models, this return to stability in the $x-z$ plane causes the x-axis orbit to become stable in both directions, at least over a limited range in energy and in c/a (Figure 1). The axial orbit becomes unstable once again at still lower values of c/a, through the appearance of a $3:1$ resonance in the direction of

the z axis (Figure 5). In nearly prolate models, where the x-axis orbit is also unstable to perturbations in the $x-y$ plane, the appearance of the $x-z$ anti-banana orbit leaves the x-axis orbit still unstable to perturbations in the y direction (Figure 1).

At very low values of c/a, the stability of the x-axis orbit varies in a rapid and complex manner with energy and with γ, as resonances of higher and higher order occur.

The y-axis orbit (Figure 2) is unstable at almost all energies in the full range of models investigated here. Instability in the x-direction is expected due to the $1:1$ resonance that generates the $x-y$ loops; these orbits – and their associated family, the short-axis tubes – are present almost universally in Dehnen's models. As c/a decreases, the y-axis orbit also becomes unstable through the $2:1$ bifurcation that produces the $y-z$ bananas; the y-axis orbit is then unstable in both directions. At still greater model elongations, the y-axis orbit returns briefly to stability in the z-direction through the appearance of the $y-z$ anti-banana.

The stability diagram of the z-axis orbit is not given here. This orbit was found to be unstable to perturbations in both the x- and y-directions for almost all values of the model parameters, due to the $1:1$ bifurcations that produce the $x-z$ and $y-z$ loops (Goodman & Schwarzschild 1981). Thus, the long-axis tube orbits – which are parented by the $y-z$ loop orbits – are almost always present in these models. The only exceptions occur at low energies in models with $c/a \lesssim 0.2$ and $\gamma \lesssim 0.5$, where the ratio of oscillation frequencies in the z- and x-directions is too great for the $1:1$ resonance to occur. The z-axis orbit is not the parent of any banana family.

In summary: only the x-axis orbit is stable over an appreciable range of model parameters. Instability first appears through the $x-z$ banana bifurcation, which occurs at progressively larger values of c/a as γ is increased. The x-axis orbit returns to stability for a narrow range of c/a values, typically around $0.2-0.4$, through the bifurcation of the $x-z$ anti-banana.

4. Banana Orbits

Banana orbits first appear as $2:1$ bifurcations from the x-axis orbit ($x-z$ and $x-y$ bananas) or the y-axis orbit ($y-z$ banana). Stability diagrams for the $x-z$ and $x-y$ bananas are shown in Figures 6 and 7. Once these orbits bifurcate from the axial orbits, they continue to exist (though not always stably) at all higher energies and all lower values of c/a, for any given value of γ and T.

The $x-z$ banana exists and is stable over the widest range of model parameters (Figure 6). It becomes unstable only in nearly-prolate models, through a vertical $2:1$ bifurcation; for example, when $T = 0.8$, instability first occurs when c/a drops below ~ 0.35. Thus, in virtually all models with axis ratios comparable to those of real elliptical galaxies, either the x-axis orbit or the $x-z$ banana orbit is stable and can act as the parent of a family of regular boxlets.

The $x-y$ banana exists only in relatively prolate and elongated models, in which the $x-y$ frequency ratio can exceed $2:1$ (Figure 7). For moderate values of c/a, however, the $x-y$ banana is generally vertically unstable; its instability follows closely that of the $x-$axis orbit in the z-direction (Figure 1). For smaller values of c/a, e.g. $c/a \lesssim 0.5$ for $T = 0.8$, the $x-y$ banana returns to stability via a $2:1$ bifurcation at approximately the same model parameters where the $x-$axis orbit also becomes stable in the $z-$direction (Figure 8).

The $y-z$ banana was found to be almost universally unstable in the vertical (x) direction, mimicking the x-instability of the y-axis orbit.

The regular orbits associated with the $x-z$ bananas are known to be heavily populated in self-consistent triaxial models with cusps (e.g. Schwarzschild 1993; Merritt & Fridman 1996). However their usefulness is limited by the fact that the banana orbits become more strongly curved as c/a decreases, so that in sufficiently elongated models, the boxlets associated with the $x-z$ bananas are all rounder than the model figure. Figure 9 shows the value of c/a at which the $x-z$ banana has an elongation – defined as $|z_{max}/x_{max}|$, the ratio of its extent in the z and x directions – that just matches that of the model. Figure 9 suggests that the boxlets associated with the $x-z$ banana will be useful in reconstructing triaxial models for $c/a \gtrsim 0.4$.

In summary: the $x-z$ banana exists and is stable for the widest range of model parameters. It is slender enough to match the shape of the model when $c/a \gtrsim 0.4$. The $x-y$ and $y-z$ bananas either do not exist, or are vertically unstable, in all models with moderate values of c/a; the $x-y$ banana returns to stability only in highly elongated, nearly prolate models.

5. Fish Orbits

Fish orbits first appear as $3:2$ bifurcations from the x-axis orbit ($x-z$ and $x-y$ fish) or the y-axis orbit ($y-z$ fish). Stability diagrams for the $x-z$ and $x-y$ fish are shown in Figures 10 and 11. Once these orbits bifurcate from the axial orbits, they continue to exist at all higher energies and all lower values of c/a, for any given value of γ and T.

The $x-z$ fish exists and is stable in models with moderate values of c/a (Figure 10). In nearly oblate models, the $x-z$ fish first becomes unstable to perturbations in the orbital plane, while for strongly triaxial and prolate models, instability first appears in the vertical (y) direction (Figure 12). However this orbit exists stably over a substantially narrower range of model parameters than the $x-z$ banana.

The $x-y$ fish is only important in strongly prolate models (Figure 11). In strongly triaxial and oblate models, it either does not exist, or is generally unstable to vertical (z) perturbations.

The $y-z$ fish was found to be unstable to vertical perturbations for almost all values of the model parameters.

In summary: the $x-z$ fish is important in moderately flattened, oblate/triaxial models, while the the $x-y$ fish is important in highly prolate models. In strongly triaxial models, instability in both families first occurs in the vertical direction. Neither orbit exists stably for as wide a range of model parameters as the $x-z$ banana.

6. Discussion

Our results highlight the sensitivity of boxlike orbits to small changes in the central density structure of a triaxial galaxy. The range of model shapes for which the x-axis orbit – the progenitor of the box orbits – is stable becomes rapidly narrower as the cusp slope γ approaches one. For $\gamma \gtrsim 0.8$, only triaxial models with moderate axis ratios, $c/a \gtrsim 0.75$, contain stable long-axis orbits at most energies. Regular box orbits may nevertheless be present in the majority of bright elliptical galaxies, since the distribution of intrinsic shapes of these galaxies is strongly peaked at $c/a \approx 0.8$ (Tremblay & Merritt 1996), and many ellipticals have cusp slopes $\gamma \lesssim 0.8$ (Merritt & Fridman 1995; Gebhardt et al. 1996).

Of the remaining families of boxlets investigated here, those lying in the $x-z$ plane were found to be most important, in the sense that they exist and are stable in models with the widest variety of cusp slopes and axis ratios. In particular, the $x-z$ bananas are unstable only in highly flattened, nearly prolate models, and they are often more elongated than the model figure, making them useful building-blocks for a self-consistent galaxy. The boxlets in the $x-y$ and $y-z$ planes are almost always vertically unstable in strongly triaxial models (when they exist), and it seems unlikely that they could play an important role in maintaining triaxiality in real galaxies.

We have investigated only motion in the principal planes. Other resonant orbits –

although generally of a higher order – exist outside of the principal planes. Merritt & Fridman (1996) cataloged the orbits in a single triaxial model with Dehnen's density law, $\gamma = 1$, $c/a = 0.5$ and $T = 0.5$. Their Figure 4 confirms that only the $x - z$ banana and the $x - z$ fish, among the closed boxlets investigated here, are generators of regular orbit families. The $x - y$ pretzel was also found to be important at low energies, as were a number of higher-order resonances outside of the principal planes, including the $4 : 5 : 7$, $5 : 6 : 8$, and $6 : 7 : 9$ closed boxlets.

Although instability does not imply stochasticity, unstable resonant orbits are often associated with chaos. We expect that the phase space surrounding many of the unstable boxlets is stochastic. However, the timescale over which the stochasticity manifests itself in the orbital motion is likely to be a strong function of the model parameters, particularly the cusp slope γ and the energy. We will return to this question in a future study.

This work was supported by NSF grant AST 90-16515 and by NASA grant NAG 5-2803.

REFERENCES

Broucke, R. 1969, JAIAA, 7, 1003

Dehnen, W. 1993, MNRAS, 265, 250

de Zeeuw, P. T. & Lynden-Bell, D. 1985, MNRAS, 215, 713

Ferrarese, L., van den Bosch, F. C., Ford, H. C., Jaffe, W., & O'Connell, R. W. 1994, AJ, 108, 1598

Floquet, G. 1883, Ann. Scien. Ec. Norm. Sup., 12, 47

Gebhardt, K. *et al.* 1996, AJ, 112, 105

Gerhard, O. E. & Binney, J. J. 1985, MNRAS, 216, 467

Goodman, J. & Schwarzschild, M. 1981, ApJ, 245, 1087

Hairer, E., Nørsett, S. P., & Wanner, G. 1987, Solving Ordinary Differential Equations I: Nonstiff Problems (Springer: Berlin)

Heiligman, G. & Schwarzschild, M. 1979, ApJ, 233, 872

Hénon, M. 1982, Physica5D, 412

Hernquist, L. 1990, ApJ, 356, 359

Jaffe, W. 1983, MNRAS, 202, 995

Kormendy, J. 1985, ApJ, 292, L9

Kormendy, J. & Richstone, D. O. 1995, ARA&A, 33, 581

Kuzmin, G. G. 1973, in The Dynamics of Galaxies and Star Clusters, ed. T. B. Omarov (Nauka of the Kazakh S. S. R., Alma-Ata), 71.

Lauer, T. R. et al. 1992, AJ, 103, 703

Lauer, T. R., et al. 1995, AJ, 110, 2622

Lees, J. F. & Schwarzschild, M. 1992, ApJ, 384, 491

Liapunov, A. 1892, Ann. Math. Studies, 17

Magnenat, P. 1982, A& A, 108, 89

Merritt, D. & de Zeeuw, T. 1982, ApJ, 267, L19

Merritt, D. & Fridman, T. 1995, A. S. P. Conf. Ser. Vol. 86, Fresh Views of Elliptical Galaxies, ed. A. Buzzoni, A. Renzini & A. Serrano (Provo: Astronomical Society of the Pacific), 13

Merritt, D. & Fridman, T. 1996, ApJ, 460, 136

Miralda-Escudé, J. & Schwarzschild, M. 1989, ApJ, 339, 752

Papaphilippou, Y. & Laskar, J. 1997, preprint

Pfenniger, D. 1984, A& A, 134, 373

Schwarzschild, M. 1979, ApJ, 232, 236

Schwarzschild, M. 1993, ApJ, 409, 563

Tremblay, B. & Merritt, D. 1996, AJ, 111, 2243

This preprint was prepared with the AAS LaTeX macros v4.0.

Fig. 1.—

Stability diagram for the x-axis orbit. • stable; + unstable in the direction of the y axis; × unstable in the direction of the z axis; · unstable in both directions.

Fig. 2.—

Stability diagram for the y-axis orbit. + unstable in the direction of the x axis; × unstable in the direction of the z axis; · unstable in both directions.

Fig. 3.—

Stability region for the x-axis orbit. Solid lines correspond to models in which the x-axis orbit is just unstable, at the half-mass radius (shell 10), to bifurcation of the $x-z$ banana orbit. Box orbits do not exist outside the half-mass radius in models below these lines.

Fig. 4.—

Stability characteristics of the x-axis orbit when perturbed in the z-direction, for $c/a = 0.6$ and $T = 0.5$. Frequencies and e-folding rates are expressed in units of the orbital frequency. Bifurcation of the $x-z$ banana orbit occurs at successively lower energies as the cusp slope γ is increased.

Fig. 5.—

Stability characteristics of the x-axis orbit when perturbed in the z-direction, for $\gamma = 0.4$ and $T = 0.5$. Frequencies and e-folding rates are expressed in units of the orbital frequency. The x-axis orbit returns to stability through bifurcation of the $x-z$ anti-banana orbit.

Fig. 6.—

Stability diagram for the $x-z$ banana orbit. • stable; × vertically unstable. No symbol indicates that the $x-z$ banana does not exist.

Fig. 7.—

Stability diagram for the $x-y$ banana orbit. • stable; × vertically unstable. No symbol indicates that the $x-y$ banana does not exist.

Fig. 8.—

Stability characteristics of the $x-y$ banana orbit when perturbed in the z-direction,

for $\gamma = 0.6$ and $T = 0.8$. Frequencies and e-folding rates are expressed in units of the orbital frequency.

Fig. 9.—

Value of c/a at which the elongation of the $x - z$ banana matches that of the model, for $T = 0.5$, and for four values of the cusp slope: $\gamma = 0.2, 0.4, 0.6, 0.8$.

Fig. 10.—

Stability diagram for the $x - z$ fish orbit. • stable; + unstable in the plane; × vertically unstable. No symbol indicates that the $x - z$ fish does not exist.

Fig. 11.—

Stability diagram for the $x - y$ fish orbit. • stable; + unstable in the plane; × vertically unstable. No symbol indicates that the $x - y$ fish does not exist.

Fig. 12.—

Stability characteristics of the $x - z$ fish orbit when perturbed in the y-direction, for $\gamma = 0.8$ and $T = 0.8$. Frequencies and e-folding rates are expressed in units of the orbital frequency.

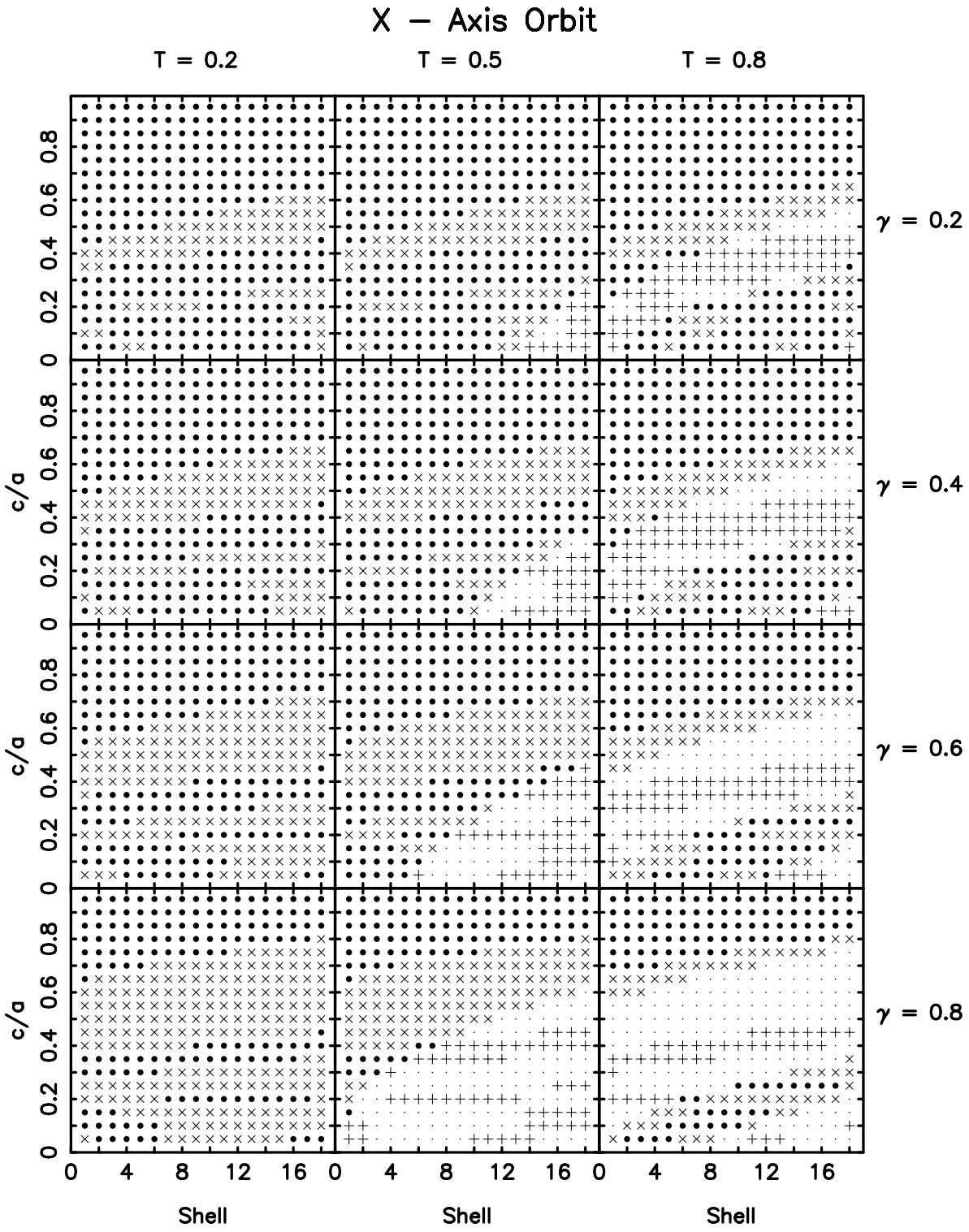
X – Axis Orbit
T = 0.2
T = 0.5
T = 0.8
γ = 0.2
γ = 0.4
γ = 0.6
γ = 0.8
c/a
0
0.2
0.4
0.6
0.8
0
4
8
12
16
Shell

Fig. 1.—

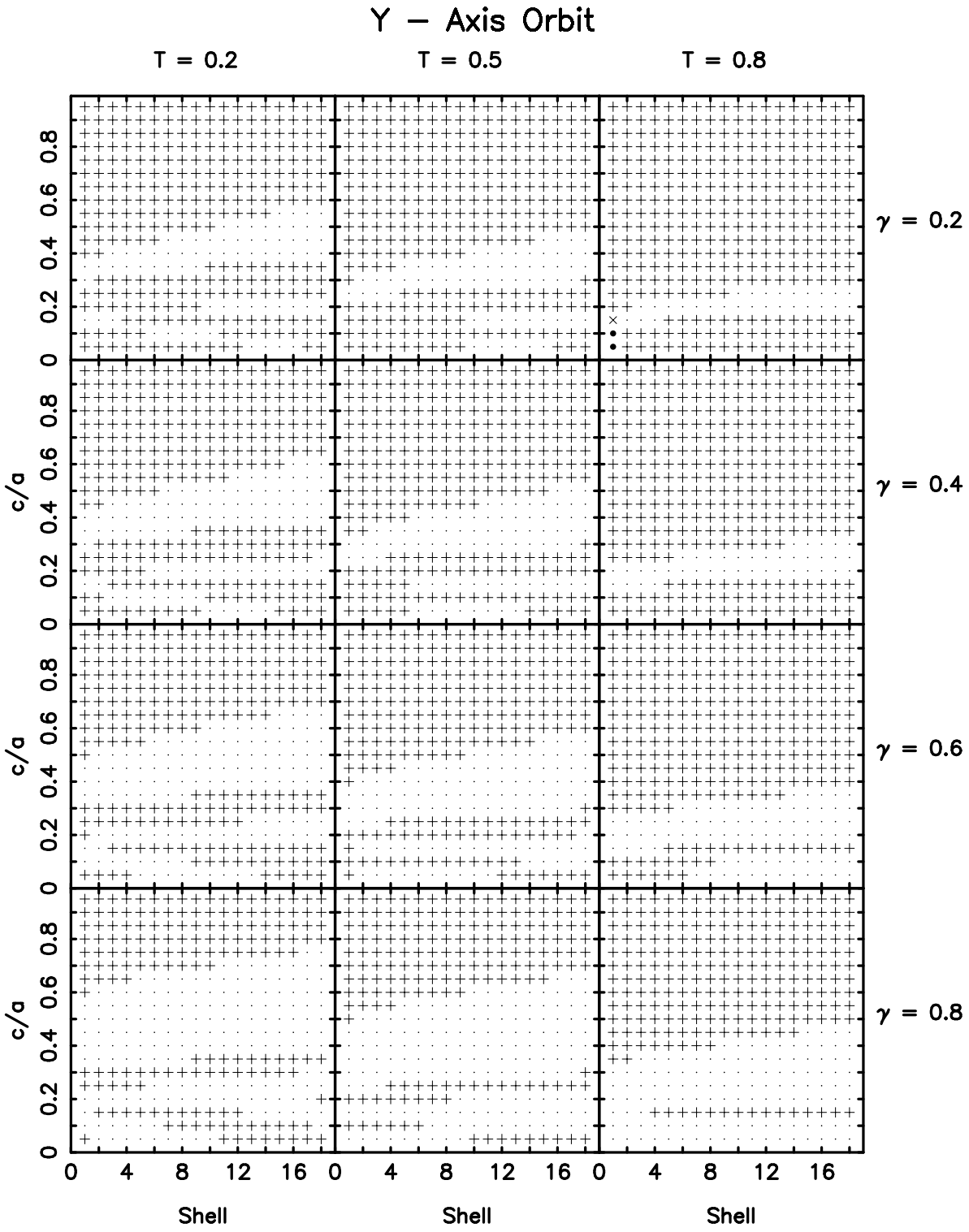
Y – Axis Orbit
T = 0.2
T = 0.5
T = 0.8
γ = 0.2
γ = 0.4
γ = 0.6
γ = 0.8
c/a
0
0.2
0.4
0.6
0.8
0
4
8
12
16
Shell

Fig. 2.—

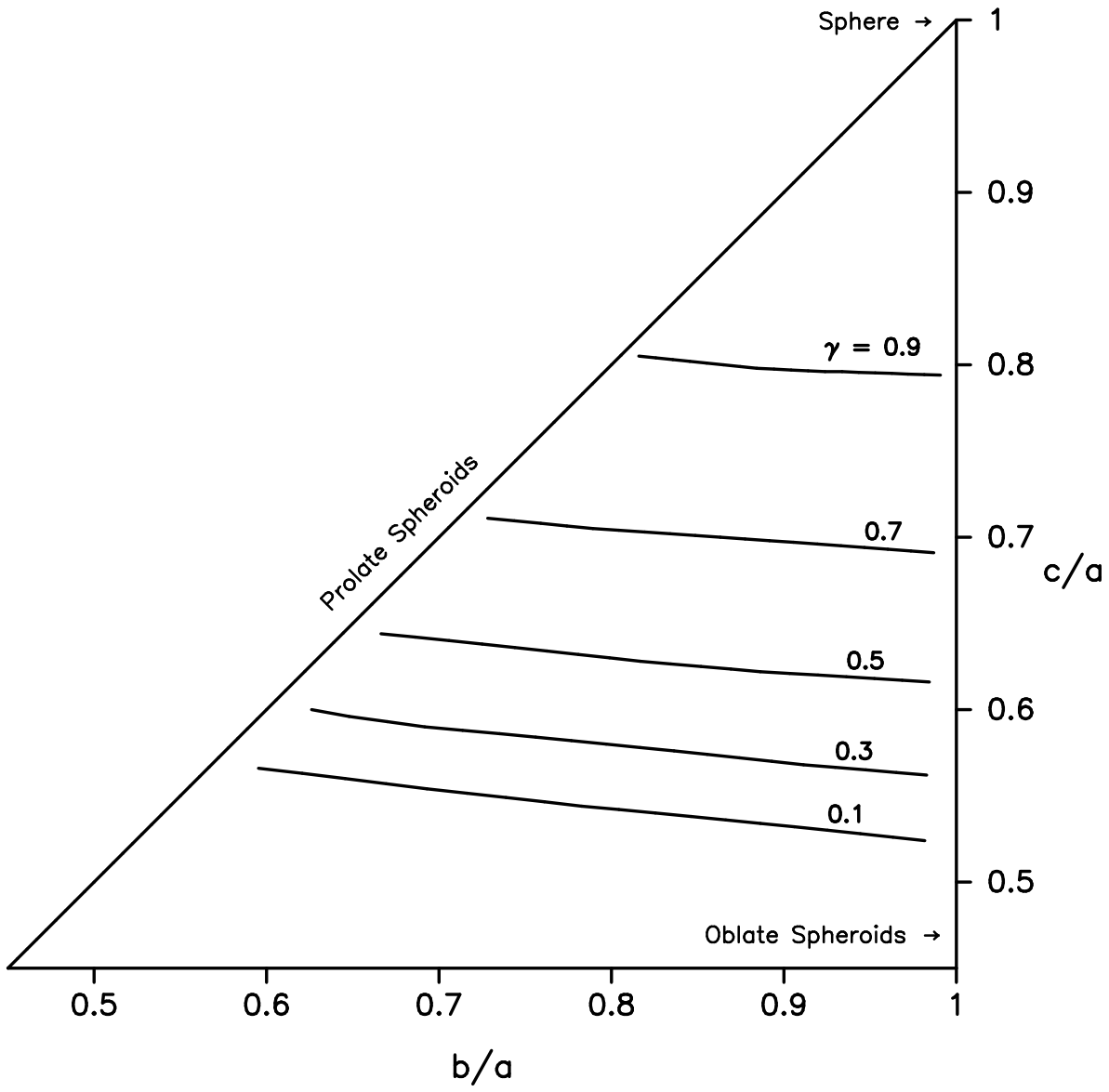
Sphere →
1
0.9
γ = 0.9
0.8
Prolate Spheroids
0.7
0.7
c/a
0.5
0.6
0.3
0.1
0.5
Oblate Spheroids →
0.5
0.6
0.7
0.8
0.9
1
b/a

Fig. 3.—

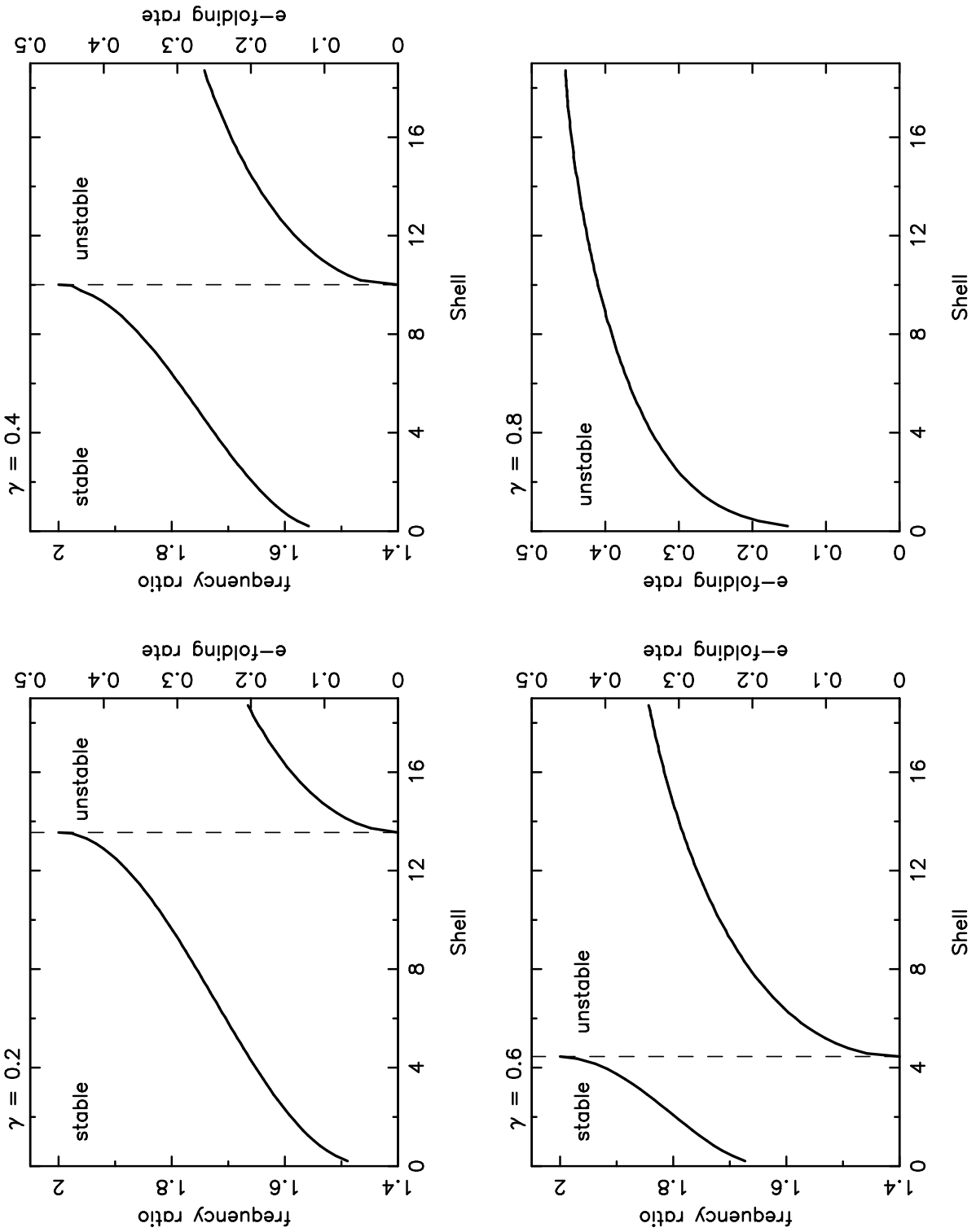
γ = 0.2
stable
unstable
frequency ratio
e–folding rate
Shell
γ = 0.4
stable
unstable
frequency ratio
e–folding rate
Shell
γ = 0.6
stable
unstable
frequency ratio
e–folding rate
Shell
γ = 0.8
unstable
e–folding rate
Shell

Fig. 4.—

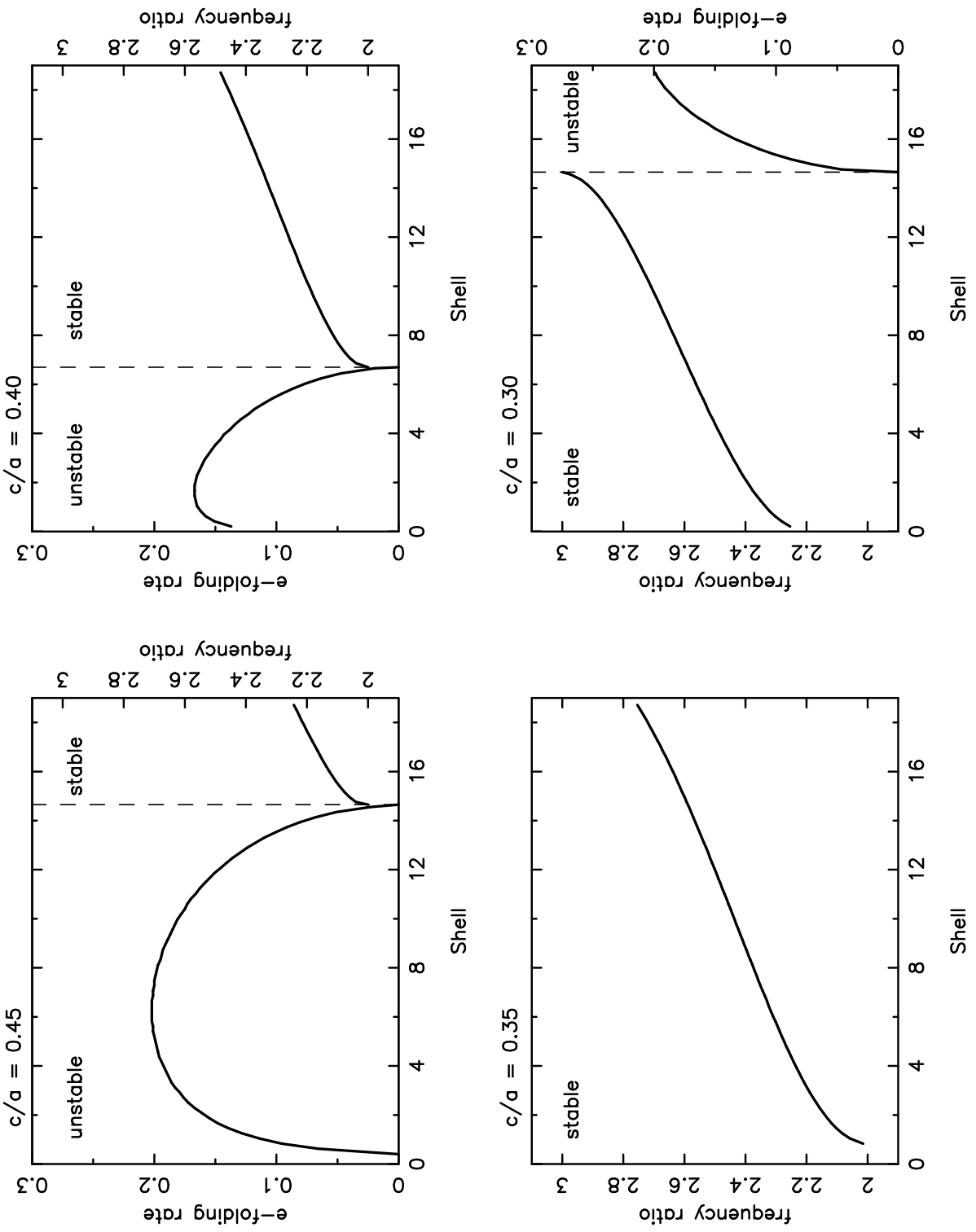
c/a = 0.45
unstable
stable
e–folding rate
frequency ratio
Shell
c/a = 0.40
unstable
stable
e–folding rate
frequency ratio
Shell
c/a = 0.35
stable
frequency ratio
Shell
c/a = 0.30
stable
unstable
e–folding rate
frequency ratio
Shell

Fig. 5.—

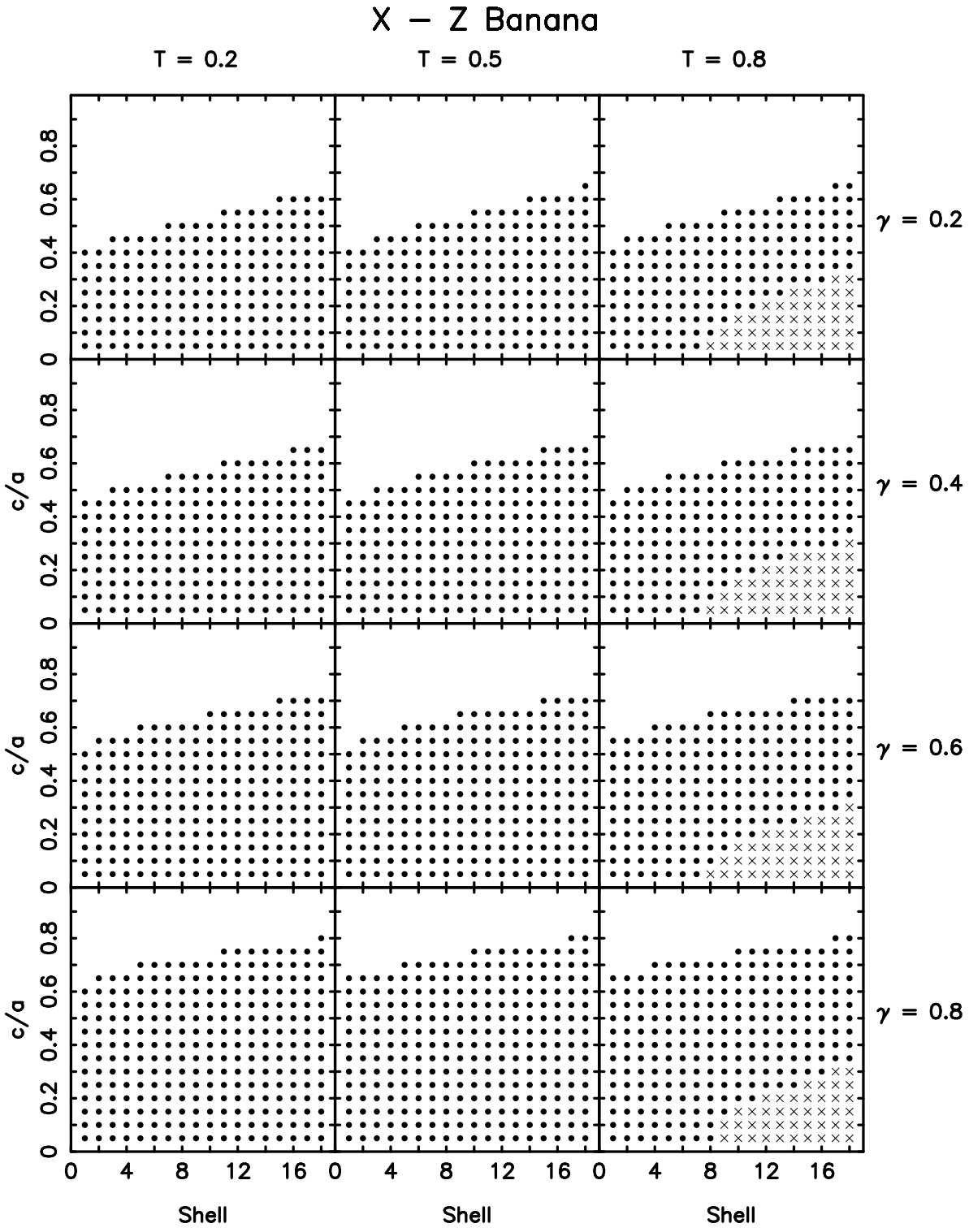
X – Z Banana
T = 0.2
T = 0.5
T = 0.8
γ = 0.2
γ = 0.4
γ = 0.6
γ = 0.8
c/a
0
0.2
0.4
0.6
0.8
0
4
8
12
16
Shell

Fig. 6.—

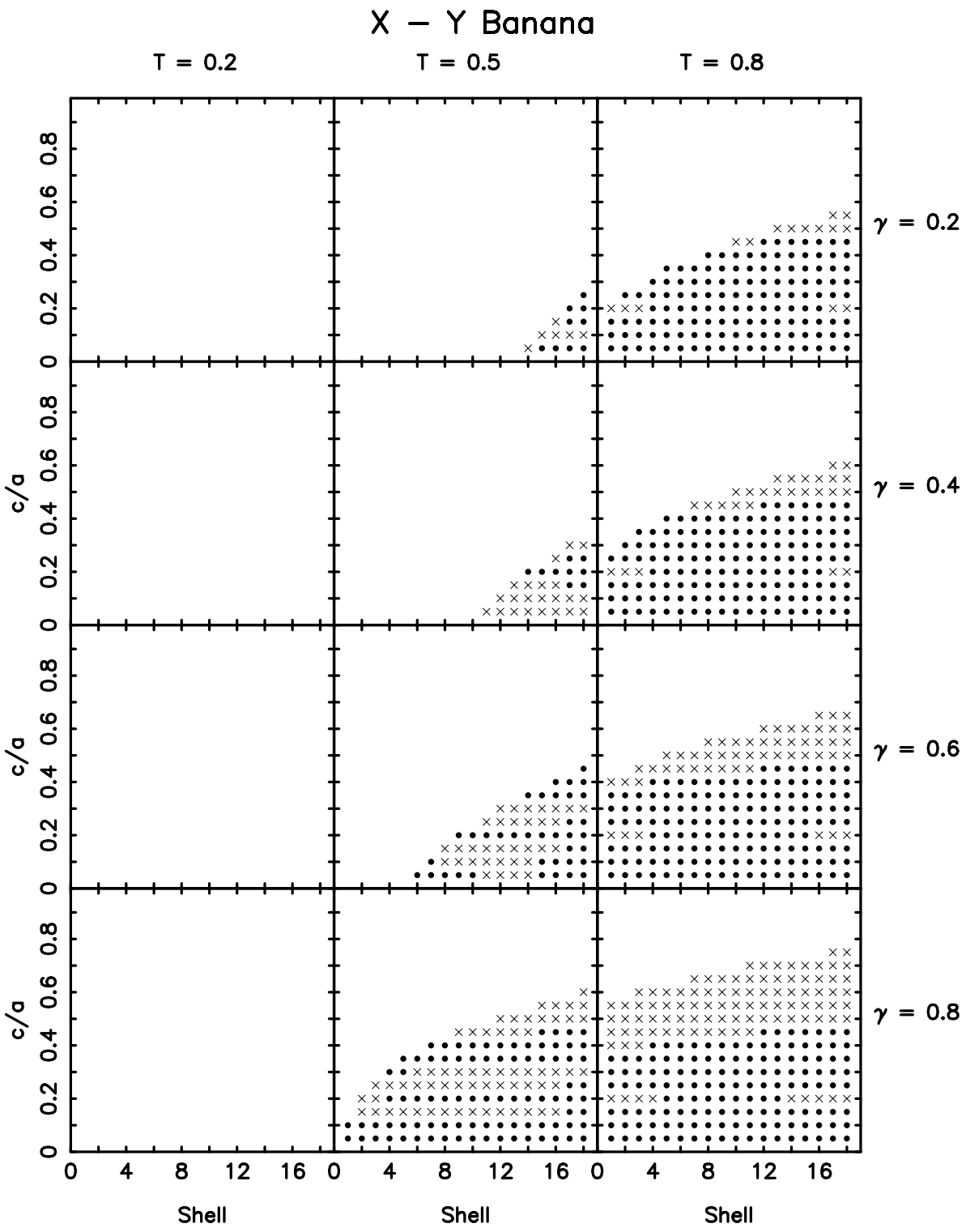
X – Y Banana
T = 0.2
T = 0.5
T = 0.8
γ = 0.2
γ = 0.4
γ = 0.6
γ = 0.8
c/a
Shell
0
0.2
0.4
0.6
0.8
4
8
12
16

Fig. 7.—

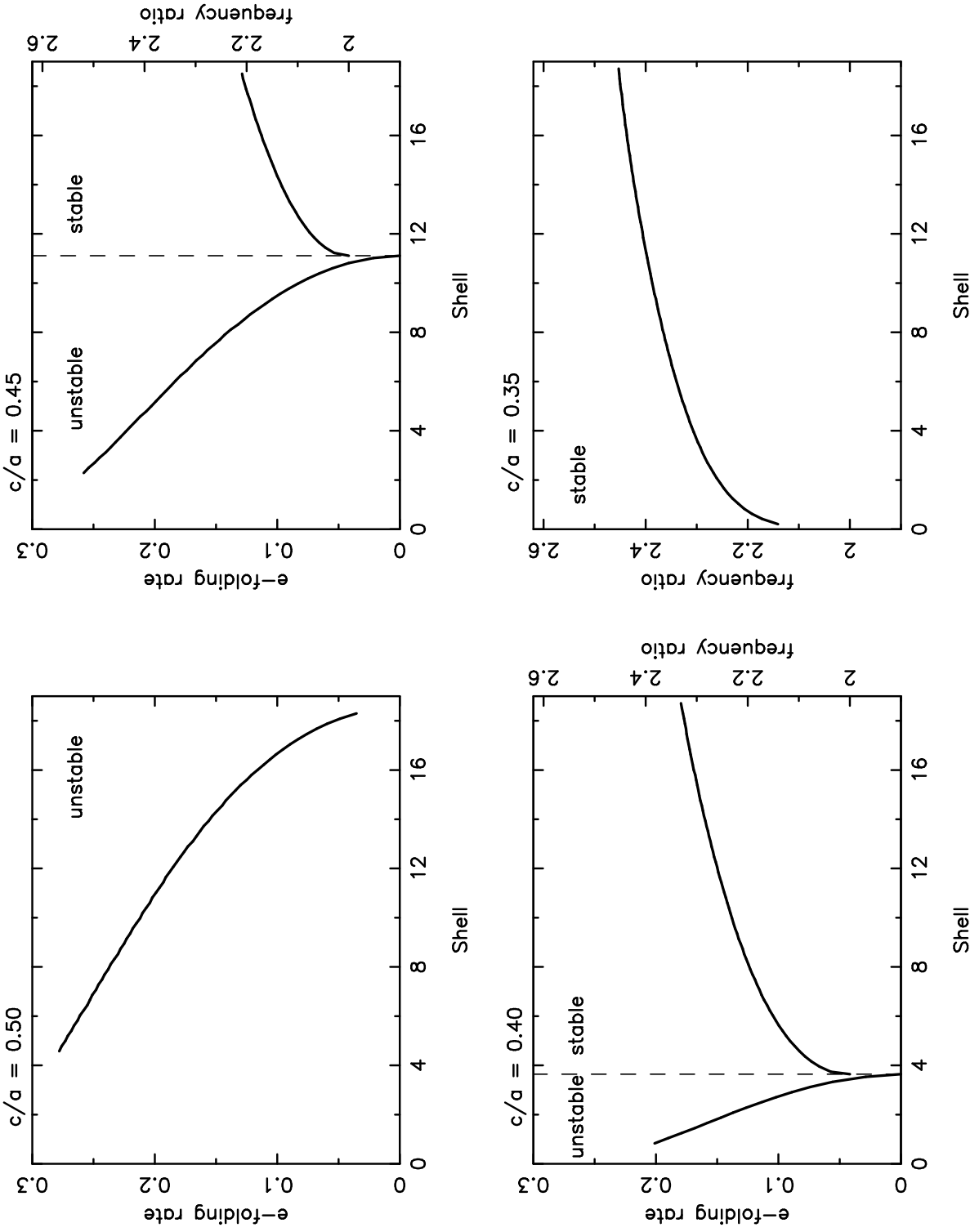
c/a = 0.45
unstable
stable
e–folding rate
frequency ratio
Shell
c/a = 0.35
stable
frequency ratio
Shell
c/a = 0.50
unstable
e–folding rate
Shell
c/a = 0.40
unstable
stable
e–folding rate
frequency ratio
Shell

Fig. 8.—

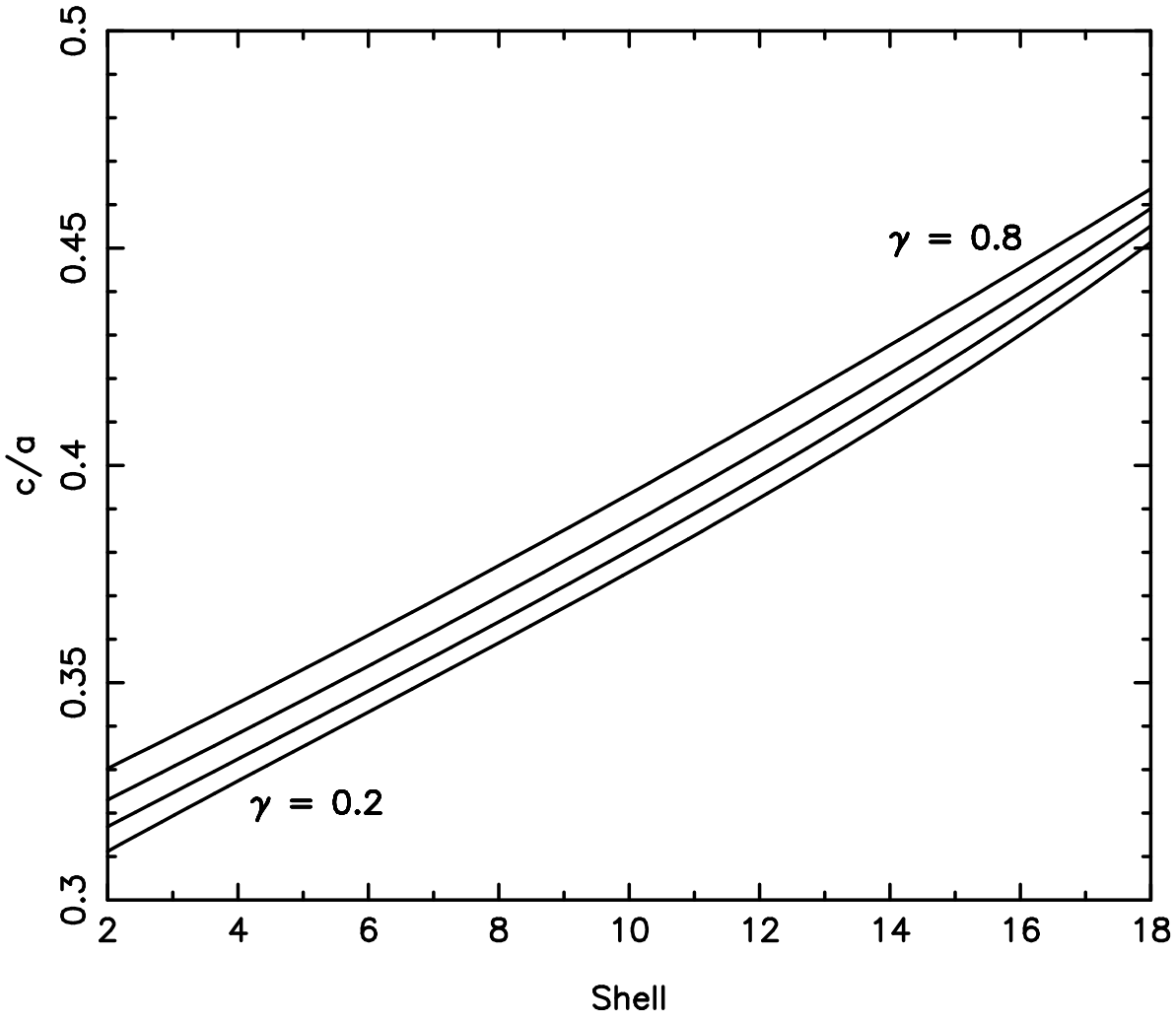

Fig. 9.—

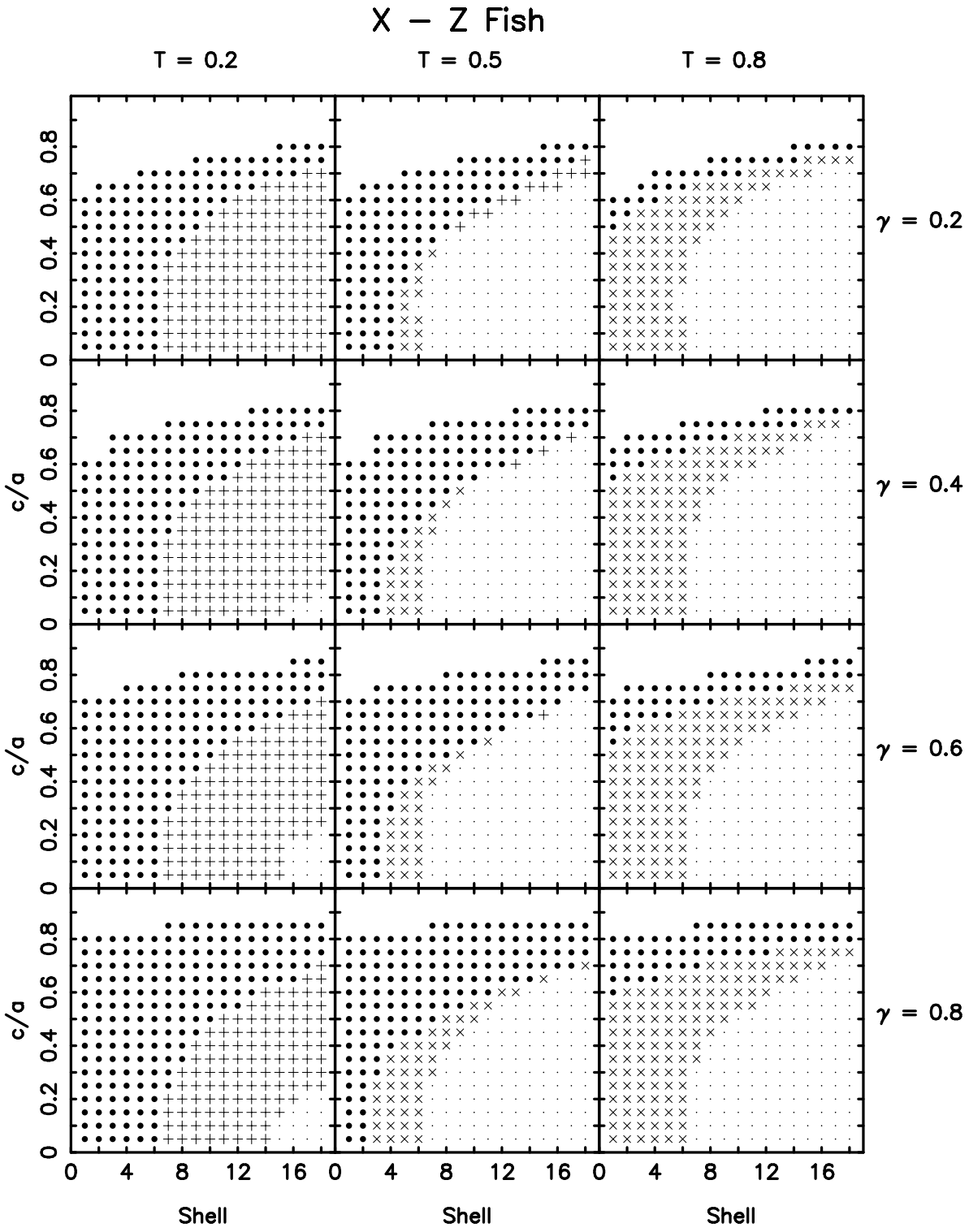
X – Z Fish
T = 0.2
T = 0.5
T = 0.8
γ = 0.2
γ = 0.4
γ = 0.6
γ = 0.8
c/a
0
0.2
0.4
0.6
0.8
0
4
8
12
16
Shell

Fig. 10.—

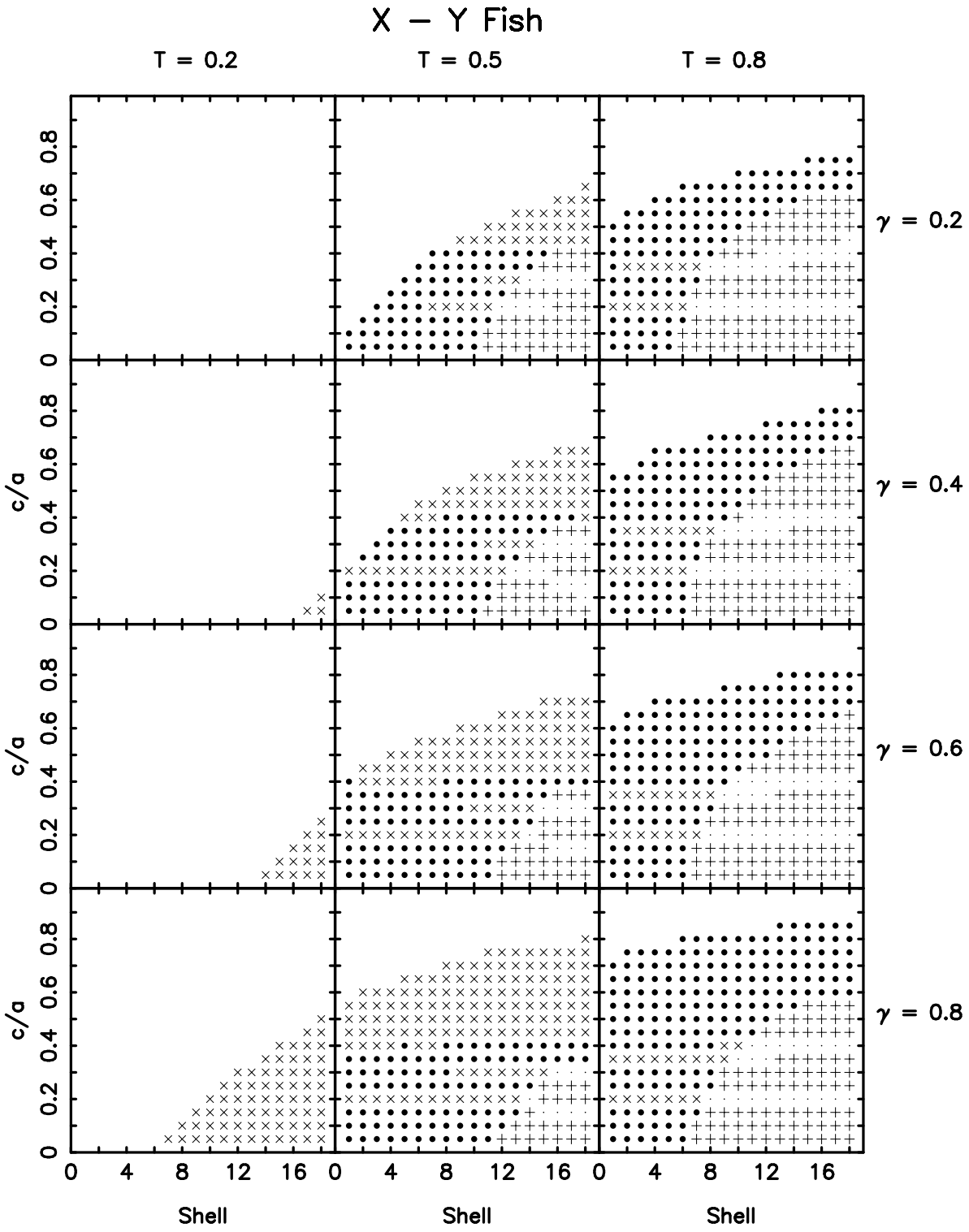
X – Y Fish
T = 0.2
T = 0.5
T = 0.8
γ = 0.2
γ = 0.4
γ = 0.6
γ = 0.8
c/a
0
0.2
0.4
0.6
0.8
0
4
8
12
16
Shell

Fig. 11.—

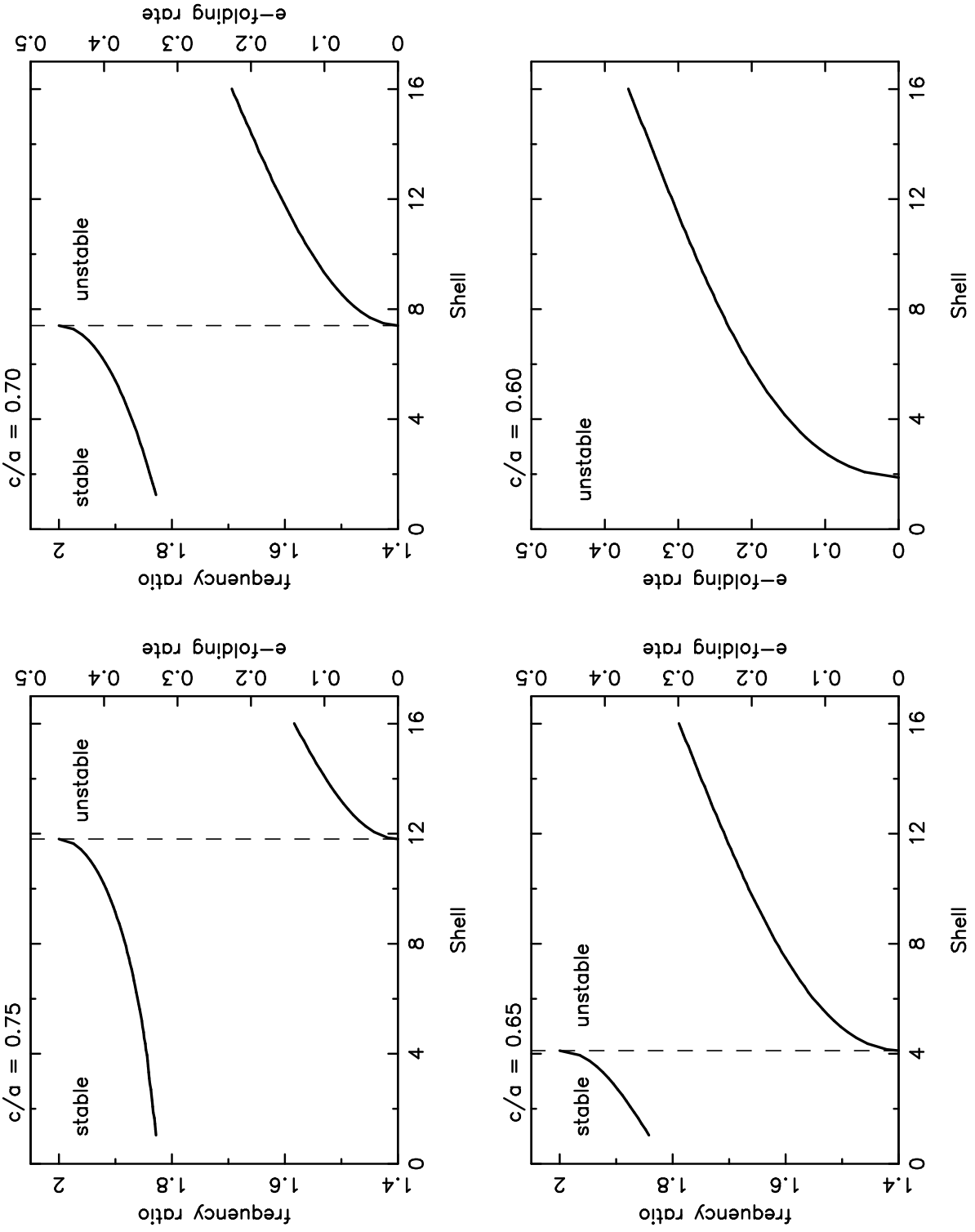
c/a = 0.75
stable
unstable
frequency ratio
e–folding rate
Shell
c/a = 0.70
stable
unstable
frequency ratio
e–folding rate
Shell
c/a = 0.65
stable
unstable
frequency ratio
e–folding rate
Shell
c/a = 0.60
unstable
e–folding rate
Shell

Fig. 12.—